Phase Transition of Electrooxidized Fe_3O_4 to γ and α-Fe_2O_3 Nanoparticles Using Sintering Treatment

I. Kazeminezhad* and S. Mosivand

Physics Department, Faculty of Science, Shahid Chamran University, Ahvaz, Iran

(Received June 4, 2013; in final form January 1, 2014)

In this work, electrosynthesis of Fe_3O_4 nanoparticles was carried out potentiostatically in an aqueous solution of $C_4H_{12}NCl$ which acts as supporting electrolyte and electrostatic stabilizer. γ-Fe_2O_3 nanoparticles were synthesized by controlling oxidation of the electrooxidized Fe_3O_4 nanoparticles at different temperature. Finally the phase transition to α-Fe_2O_3 nanoparticles was performed at high temperatures using sintering treatment. The synthesized particles were characterized using X-ray diffraction, Fourier transformation, infrared scanning electron microscopy with energy dispersive X-ray analysis, and vibrating sample magnetometry. Based on the X-ray diffraction results, the transition from Fe_3O_4 to cubic and tetragonal γ-Fe_2O_3 was performed at 200 °C and 650 °C, respectively. Furthermore, phase transition from metastable γ-Fe_2O_3 to stable α-Fe_2O_3 with rhombohedral crystal structure was approved at 800 °C. The existence of the stabilizer molecules at the surface of Fe_3O_4 nanoparticles was confirmed by Fourier transformation infrared spectroscopy. According to scanning electron microscopy images, the average particles size was observed around 50 nm for electrooxidized Fe_3O_4 and γ-Fe_2O_3 nanoparticles prepared at sintering temperature lower than 900 °C, however by raising sintering temperature above 900 °C the mean particles size increases. Energy dispersive X-ray point analysis revealed that the nanoparticles are almost pure and composed of Fe and O elements. According to the vibrating sample magnetometry results, saturation magnetization, coercivity field, and remnant magnetization decrease by phase transition from Fe_3O_4 to Fe_2O_3.

DOI: 10.12693/APhysPolA.125.1210

PACS: 75.75.cd, 61.46.Df, 61.46.Bc

1. Introduction

Magnetic transition metal oxides have been the subject of several researches, because of their special properties, such as superconductivity and phase transitions. Iron oxides nanoparticles are reported as applicable materials owning to their unique magnetic and electronic properties. Due to chemical stability, biocompatibility of maghemite nanoparticles, ferrofluids of γ-Fe_2O_3 nanoparticles can be used for magnetic fluid hyperthermia (MFH) in tumor treatment and also in medicine [1–10].

The most industrially important iron ores are iron oxides. There are well known iron oxides such as Fe_3O_4 and Fe_2O_3 in Fe–O system. Magnetite (Fe_3O_4) is a ferrimagnetic mineral and a member of the spinel group. It is sometimes formulated as Fe_3O_4 involving one part FeO and one part Fe_2O_3 and has a cubic inverse spinel structure with Fe^{3+} ions at A sites (tetrahedral coordination) and (Fe^{2+}, Fe^{3+}) ions at B sites (octahedral coordination). Iron(III) oxide is known as hematite (α-Fe_2O_3) or maghemite (γ-Fe_2O_3). Hematite is the most stable iron oxide under ambient conditions with rhombohedral, corundum (α-Al_2O_3) structure with black color to steel-gray, or brown to red. Magnetic properties of hematite are dependent on many factors such as pressure, particle size, and magnetic field intensity. Hematite which is an important n-type semiconductor ($E_g = 2.1$ eV) under ambient conditions, has found many technological applications. Maghemite has the same structure as Fe_3O_4, it is spinel ferrite and converts to the alpha phase at high temperatures. There are different ways to synthesis of Fe_2O_3 nanoparticles such as thermal oxidation of iron, reactive sputtering of Fe in the presence of O_2, and chemical vapor deposition of iron compounds. It can be also produced from sputtering or powder sintering [11–16].

To date, several different methods have been used to synthesis of Fe_3O_4 nanoparticles including ball milling [17], chemical precipitation [18, 19] and thermal decomposition [20]. Recently, electrooxidation method synthesis has begun to fabricate some of oxidized nanoparticles. One of the best advantages of this method is to control the particles size by controlling the growth parameter such as growth temperature or applied potential [21].

The goal of this research is the synthesis of Fe_3O_4 nanoparticles by simple and inexpensive electrooxidation method and preparation of γ and α Fe_2O_3 phases by sintering treatment of Fe_3O_4 and to study their magnetic structural and optical properties.

2. Experimental

Fe_3O_4 nanoparticles were synthesized by electrooxidation of iron in aqueous solution containing an electrostatic stabilizer using a chronoamperometry technique [10]. A 0.04 M $C_4H_{12}NCl$ (Merck) solution was used as both supporting electrolyte and organic coating agent. Two iron plates 1 cm × 1 cm and 1 cm ×

*corresponding author; e-mail: I.Kazeminezhad@scu.ac.ir

4 cm (> 99.9%) were purchased from Alfa Aesar and used as anode and cathode, respectively. The electrodes were polished by fine grain emery paper and cleaned with ethanol. Two cleaned electrodes were placed by a distance of 1 cm apart from each other. After applying an appropriate potential between the electrodes, the chemical reactions take place and Fe_3O_4 clusters are beginning to form in the electrolyte. When the chemical reaction occurs the colorless solution turns to yellow, brown-red, and subsequently to black indicating the formation of Fe_3O_4. The black precipitate was separated from the electrolyte solution using an external magnetic field, cleaned by three cycles of separation/washing/redispersion in deionized water, and then dried at constant temperature.

In order to prepare γ-Fe_2O_3 and α-Fe_2O_3 nanoparticles the obtained black powders have been sintered at different temperatures ranging from 100 °C to 1000 °C for 4 h. It was observed that the color changed from black, to brown, red, and grey. In fact, the color of the black powder did not change at 100 °C, but it changed to dark brown, light brown, reddish-brown, red, and grey at 150 °C and 200 °C, up to 550 °C, 650 °C, 800 °C, and 900 °C, respectively. The difference between the colors is due to different phases of iron oxide.

The crystal structure of the products was determined by a PW1840 X-ray diffractometer (XRD) using Cu K_α radiation ($\lambda = 1.5405$ Å) generated at 40 kV and 30 mA. A Leo transmission electron microscope (TEM) model 912 AB and a LEO scanning electron microscope (SEM/EDX) model 1455 VP were employed to study the morphology, particle size, and nanostructure of the iron oxide particles. Magnetic measurements at room temperature were conducted using a home-made vibrating sample magnetometer (VSM) method. A Perkin Elmer Fourier transformation infrared (FT-IR) spectroscope model LX185256 was employed to provide information about the interaction between the organic molecules and the iron oxide surface.

3. Results and discussion

3.1. Mechanism of formation of Fe_3O_4, γ-Fe_2O_3 and α-Fe_2O_3 nanoparticles

The formation mechanism of Fe_3O_4 nanoparticles was investigated by pH measurement and analysis of intermediate products. The data shows that the pH is 5.4 at the beginning of the reaction. A few minute after applying cell potential pH increases up to 9.5 and then decreases to 8.3. Formation mechanism of Fe_3O_4 nanoparticles by electrooxidation can be speculated as below [21]: at the beginning of the reaction, Fe was oxidized first to ferrous and then to ferric ions (1 and 2):

$$\mathrm{Fe} \Leftrightarrow \mathrm{Fe}^{2+} + 2\mathrm{e}^-, \tag{1}$$

$$\mathrm{Fe}^{2+} \Leftrightarrow \mathrm{Fe}^{3+} + 1\mathrm{e}^-, \tag{2}$$

electrolysis of water is another reaction that takes place and provides protons around the anode (3):

$$\mathrm{H_2O} \Leftrightarrow 2\mathrm{H}^+ + 2\mathrm{e}^- + \frac{1}{2}\mathrm{O_2}; \tag{3}$$

reduction of water takes place around the cathode as (4):

$$2\mathrm{H_2O} + 2\mathrm{e}^- \Leftrightarrow \mathrm{H_2} + 2\mathrm{OH}^-. \tag{4}$$

When reaction (4) occurs, pH increases up to 9.5. The amount of OH^- ions present in solution increases and pH and subsequently in such conditions. Brown color solution (ferric hydroxide) occurs during the reaction (5)

$$\mathrm{Fe}^{3+} + 3\mathrm{OH}^- \Leftrightarrow \mathrm{Fe(OH)_3(s)}. \tag{5}$$

After reduction of ferric hydroxide at the cathode Fe_3O_4 can be formed

$$3\mathrm{Fe(OH)_3(s)} + \mathrm{H}^+ + \mathrm{e}^- \Leftrightarrow \underline{\underline{\mathrm{Fe_3O_4(s)}}} + 5\mathrm{H_2O}. \tag{6}$$

To prepare γ-Fe_2O_3 and α-Fe_2O_3 nanoparticles the Fe_3O_4 black powders were sintered at different temperatures ranging from 100 °C to 1000 °C:

$$2\mathrm{Fe_3O_4} + \frac{1}{2}\mathrm{O_2} \xrightarrow{\text{heat}} 3\underline{\underline{(\gamma - \mathrm{Fe_2O_3})}}, \tag{7}$$

$$2\mathrm{Fe_3O_4} + \frac{1}{2}\mathrm{O_2} \xrightarrow{\text{heat}} 3\underline{\underline{(\alpha - \mathrm{Fe_2O_3})}}. \tag{8}$$

3.2. XRD results

Figure 1 illustrates the XRD patterns of (a) initial black powders; and sintered powders at (b) 200 °C, (c) 650 °C, and (d) 800 °C. One can see that the black powder has inverse cubic spinel structure of Fe_3O_4 (compared with JCPDS card, no. 88-0315), while by raising the temperature up to 200 °C and 650 °C, it is transited to cubic

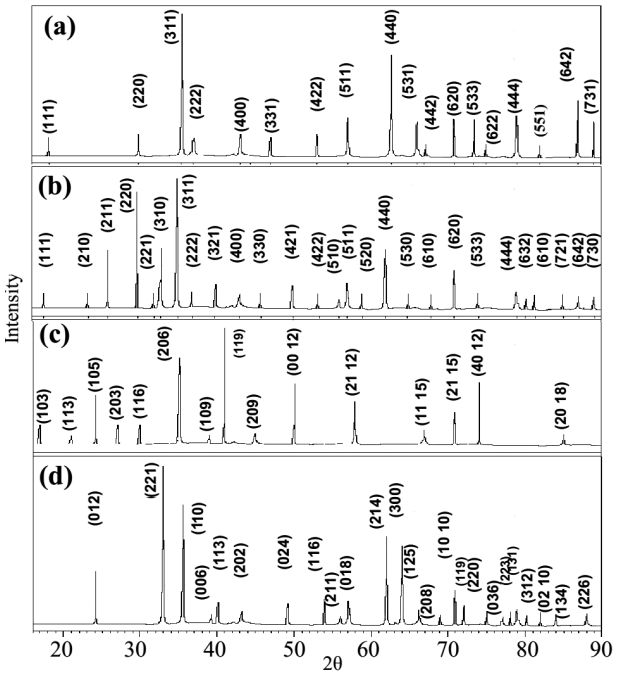

Fig. 1. XRD patterns of electrooxidized nanoparticles grown at 60 °C (a) before sintering which are Fe_3O_4; after sintering for 4 h at (b) 200 °C, (c) 650 °C, and (d) 800 °C.

and tetragonal structures of γ-Fe_2O_3, respectively (compared with JCPDS cards, no. 39-1346 and 25–1402), and finally to the complete phase of rhombohedral α-Fe_2O_3 phase at 800 °C (compared with JCPDS card, no. 87--1164). All samples prepared at different sintering treatment with their identifications are listed in Table I. According to these data, an increase in the sintering temperature led to an increase in the distinct growth orientations of crystallites for both maghemite and hematite nanoparticles.

TABLE I

All samples that were prepared at different sintering temperatures with their identifications.

Sintering temperature	Iron oxide phase	Color	Indexes of observed peaks	Compared with JCPDS cards, no.
100 °C	inverse cubic spinel structure of Fe_3O_4	black	all	88-0315
150 °C	cubic γ-Fe_2O_3(incomplete)	dark-brown	(110)(211)(220)(311)(400) (422)(511)(440)(620)(533)	39-1346
200 °C	cubic γ-Fe_2O_3	light-brown	all	39-1346
550 °C	tetragonal γ-Fe_2O_3 (incomplete)	reddish-brown	(101)(103)(113)(116)(206) (119)(00 12)(11 15) (40 12)(31 21)(51 21)	25-1402
600 °C	tetragonal γ-Fe_2O_3 (incomplete)	reddish-brown	(101)(103)(113)(116)(206) (109)(119)(00 12)(11 15) (40 12)(31 21)(51 21)	25-1402
650 °C	tetragonal γ-Fe_2O_3	reddish-brown	all	25-1402
700 °C	rhombohedral $\alpha-Fe_2O_3$ (incomplete)	red	(012)(104)(110)(113)(024) (116)(214)(300)(220)(036) (223)(31 2)(128)(02 10)	87-1164
800 °C	rhombohedral α-Fe_2O_3	red	all	87-1164
900 °C	rhombohedral α-Fe_2O_3	gray	all	87-1164
1000 °C	rhombohedral α-Fe_2O_3	gray	all	87-1164

3.3. FT-IR spectroscopy result

In order to confirm the existence of stabilizer molecules at the surface of the nanoparticles, all samples were characterized using FT-IR technique. Figure 2 shows a typical FT-IR spectrum of Fe_3O_4 particles grown at 60 °C. The spectrum can be divided into three regions, the first one goes from 3650 cm^{-1} to 3200 cm^{-1} and a band appears at 3496.3 cm^{-1} due to O–H vibrations of water. The second region from 1000 cm^{-1} to 1450 cm^{-1} corresponds to the vibrations of the surfactant molecules. In this case, a broad band at 1071.8 cm^{-1} was observed and assigned to C–N vibrations coming from the amine molecules. Finally, between the 850 cm^{-1} and 400 cm^{-1} the strong band at 571.25 cm^{-1} belonging to the stretching vibration mode of Fe–O bonds in Fe_3O_4 appears. These results are comparable to those presented by Cabrera et al. [21].

3.4. SEM/EDX analysis results

The morphology and size distribution of the iron oxide nanoparticles were determined using SEM. Four typical SEM images of Fe_3O_4, γ-Fe_2O_3 and α-Fe_2O_3 synthesized particles at different conditions are shown in Fig. 3. Based on the SEM images, the size of the Fe_3O_4 particles is in the nano range and they agglomerate into clusters, which is due to the heating of the particles during drying for SEM sample preparation and additionally due to the magnetic dipole interactions of Fe_3O_4 magnetic particles. Particles agglomeration while drying is a problem in magnetic nanoparticle systems [14].

Figure 4 illustrates the EDX point analysis of Fe_3O_4 nanoparticles. The peaks corresponding to Fe and O elements can be clearly seen. The Cl and C peaks come from the surfactant amine. The Al peak belongs to aluminum substrate which is used for preparation of SEM analysis. There is a visible peak, which corresponds to Ag layer coated on the surface of Fe_3O_4 nanoparticles for SEM imaging.

3.5. TEM/ED analysis results

The morphology, size, and electron diffraction (ED) pattern of the particles were determined by TEM. The mean particle size and distribution were determined by size average of at least 100 particles which are randomly selected on the TEM images. Figure 5 shows TEM images and corresponding ED patterns of the samples before (a) and after (b, c and d) sintering. It can be seen that all samples are mainly composed of quasi-spherical

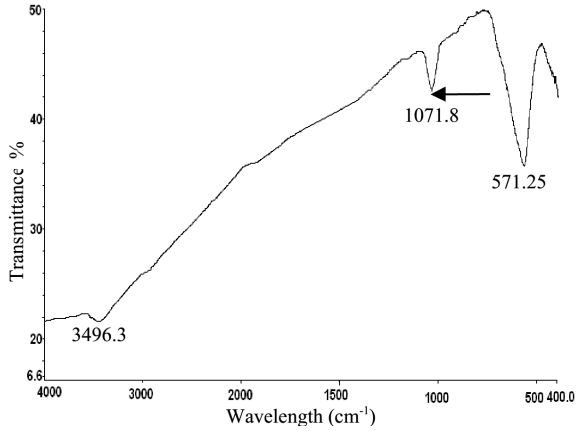

Fig. 2. FT-IR spectrum of Fe_3O_4 nanoparticles grown at 60 °C.

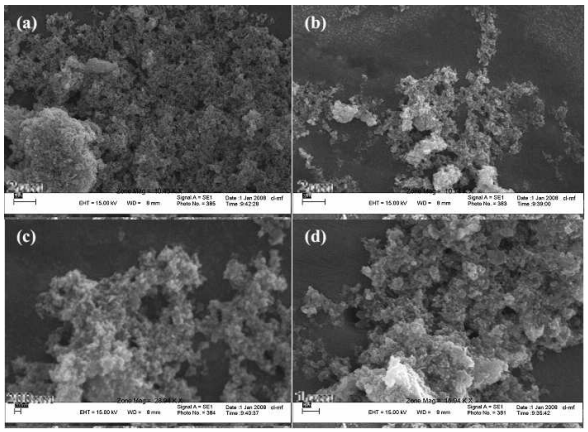

Fig. 3. SEM images of electrooxidized nanoparticles grown at $T = 60$ °C (a) before sintering which are Fe_3O_4; after sintering for 4 h at (b) 650 °C, (c) 800 °C, and (d) 1000 °C.

particles and the mean particles size increases by increasing sintering temperature above 900 °C. For example, the mean particles size for prepared sample at 1000 °C is about 70 nm (Fig. 5d). In addition, ED patterns of the particles are ring-like due to the distinct orientations of the crystallites. This result confirms that the structures of Fe_3O_4, γ-Fe_2O_3, and α-Fe_2O_3 nanoparticles are polycrystalline.

3.6. VSM results

Room temperature magnetic moments of the three different types of iron oxide nanoparticles were measured using a home-made VSM with a 1.1 T permanent magnet source. In Fig. 6 hysteresis loops of electrooxidized nanoparticles before sintering (Fe_3O_4) and after sintering at 200 °C (γ-Fe_2O_3) and 800 °C (α-Fe_2O_3) for 4 h are shown. As can be seen, the magnetic properties of

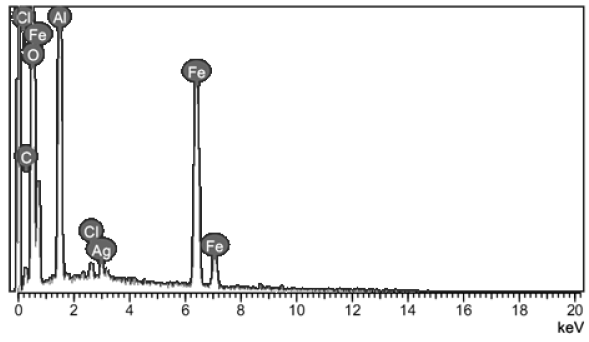

Fig. 4. EDX spectrum of electrooxidized Fe_3O_4 nanoparticles grown at 60 °C.

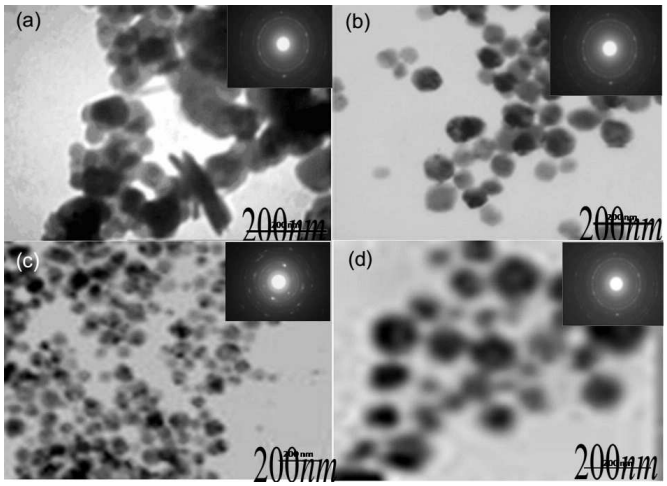

Fig. 5. TEM images and ED patterns of electrooxidized nanoparticles grown at 60 °C (a) before sintering which are Fe_3O_4; after sintering for 4 h at (b) 650 °C, (c) 800 °C, and (d) 1000 °C.

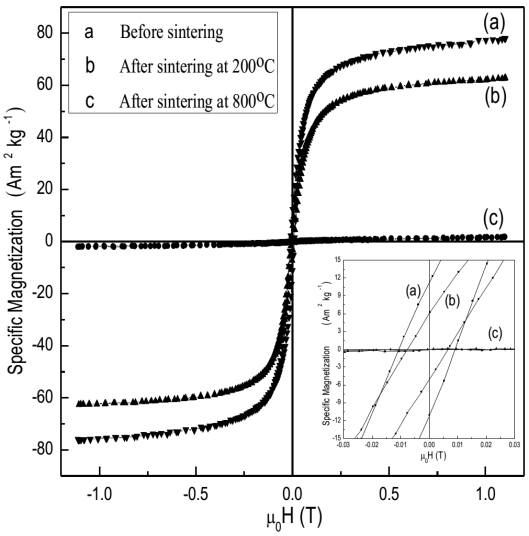

Fig. 6. Room temperature hysteresis loops of electrooxidized nanoparticles before sintering and after sintering for 4 h at 200 °C and 800 °C.

iron oxide nanoparticles change by phase transition from Fe_3O_4 to γ and α-Fe_2O_3. Some more details about saturation magnetization (M_s), coercivity force (H_c), and remnant magnetization (M_r) of the samples are presented in Table II.

TABLE II

Saturation magnetization (M_s), coercivity force (H_c), and remnant magnetization (M_r) for electrooxidized nanoparticles before sintering and after sintering for 4 h at 200 °C and 800 °C.

Sample	Sintering temperature [°C]	Saturation magnetization [A m^2 kg^{-1}]	Remnant magnetization [A m^2 kg^{-1}]	Coercivity [T]
Fe_3O_4	–	77.9	11.3	0.009
γ-Fe_2O_3	200	62.6	5.5	0.006
α-Fe_2O_3	800	1.7	0	0

4. Conclusion

The synthesis of Fe_3O_4 nanoparticles has been achieved by electrooxidation of iron in aqueous solution using potentiostatic mode. The obtained nanoparticles have been sintered at different temperatures. In this research, it was found that the sintering treatment plays an important role to control the phase structure of the products. XRD results showed that the phase transition of nanoparticles from Fe_3O_4 to cubic and tetragonal γ-Fe_2O_3 occurs at about 200 °C and 650 °C, respectively. Additionally, by increasing the sintering temperature up to 800 °C the γ-Fe_2O_3 phase transfers to α-Fe_2O_3. According to SEM images quasi-spherical iron oxide nanoparticles with the mean size of about 50 nm were formed, and also it was found that the sintering temperature is not strongly effective on size and shape of the particles for samples sintered at temperatures lower than 900 °C, however, by raising sintering temperature above 900 °C the mean particles size increases. EDX point analysis revealed that the nanoparticles are composed of Fe and O elements. According to VSM results the magnetic parameters such as M_s, M_r, and H_c, were clearly changed by increasing the sintering temperature.

Acknowledgments

The authors would like to thank Shahid Chamran University for financial support and Prof. Michael Coey (School of Physics, Trinity College Dublin) for the VSM measurements.

References

[1] H. Park, P. Ayala, M.A. Deshusses, A. Mulchandani, H. Choi, N.V. Myung, *Chem. Eng. J.* **139**, 208 (2008).

[2] K. Nishio, Y. Masaike, M. Ikeda, H. Narimatsu, N. Gokon, S. Tsubouchi, M. Hatakeyama, S. Sakamoto, N. Hanyu, A. Sandhu, H. Kawaguchi, M. Abe, H. Handa, *Coll. Surf. B Biointerfaces* **64**, 162 (2008).

[3] M.R. Khorramzadeh, Z. Esmail-Nazari, Z. Zarei-Ghaane, M. Shakibaei, K. Mollazadeh-Moghaddam, M. Iranshahi, A.R. Shahverdi, *Mater. Sci. Eng. C* **30**, 1038 (2010).

[4] H. Basti, L. Ben Tahar, L.S. Smiri, F. Herbst, M.J. Vaulay, F. Chau, S. Ammar, S. Benderbous, *J. Coll. Interface Sci.* **341**, 248 (2010).

[5] Y. Li, X. Qui, Y. Lin, X. Liu, R. Gao, A. Wang, *Appl. Surf. Sci.* **256**, 6977 (2010).

[6] J. Qu, G. Liu, Y. Wang, R. Hong, *Adv. Powder Technol.* **21**, 461 (2010).

[7] Y.F. Shen, J. Tang, Z.H. Nie, Y.D. Wang, Y. Ren, L. Zuo, *Bioresour. Technol.* **100**, 4139 (2009).

[8] J. Huang, G. Yang, W. Meng, L. Wu, A. Zhu, X. Jiao, *Biosens. Bioelectron.* **25**, 1204 (2010).

[9] Y. Wu, J. Zhang, Y. Tong, X. Xu, *J. Hazard. Mater.* **172**, 1640 (2009).

[10] I. Kazeminezhad, S. Mosivand, M. Farbod, *Curr. Nanosci.* **7**, 819 (2011).

[11] G. Cao, *Nanostructures and Nanomaterials, Synthesis, Properties and Applications*, Imperial College Press, London 2004.

[12] G. Schimanke, M. Martin, *Solid State Ionics* **136**, 1235 (2000).

[13] R.Y. Hong, T.T. Pan, Y.P. Han, H.Z. Li, J. Ding, S. Han, *J. Magn. Magn. Mater.* **310**, 37 (2007).

[14] X. Wei, R.C. Viadero Jr, *Coll. Surf. A: Physicochem. Eng. Asp.* **294**, 280 (2007).

[15] K. Tokumitsu, T. Nasu, *Scr. Mater.* **44**, 1421 (2001).

[16] H. Iida, K. Takayanagi, T. Nakanishi, T. Osaka, *J. Coll. Interface Sci.* **314**, 274 (2007).

[17] D. Chen, S. Ni, Z. Chen, *Chin. Particuol.* **5**, 357 (2007).

[18] Y.S. Liu, P. Liu, Z.X. Su, F.S. Li, F.S. Wen, *Appl. Surf. Sci.* **255**, 2020 (2008).

[19] J. Liu, B. Sun, J. Hu, Y. Pei, H. Li, M. Qiao, *J. Catal.* **274**, 287 (2010).

[20] D. Amara, I. Felner, I. Nowik, S. Margel, *Coll. Surf. A, Physicochem. Eng. Asp.* **339**, 106 (2009).

[21] L. Cabrera, S. Gutierrez, N. Menendez, M.P. Morales, P. Herrasti, *Electrochim. Acta* **53**, 3436 (2008).